Characterisation of nanoclay dispersion in resin transfer moulded glass/nanoclay/epoxy composites

L. Aktas, Y. K. Hamidi and M. C. Altan*

A novel approach for characterisation of nanoclay dispersion in polymeric composites using electron microprobe analysis (EMPA) is presented. Dispersion analysis was performed on three sets of centre-gated discs fabricated by resin transfer moulding. The first set was neat epoxy polymer without reinforcement, whereas the second set comprised 17 vol.-% randomly oriented chopped glass fibre preforms. The last set, in addition to the glass fibre reinforcement, contained 1·7 wt-% Cloisite 25A nanoclay. Upon completion of curing, a sample along the radius of a nanoclay reinforced disc was analysed on a Cameca SX50 electron microprobe analyser. The results from scanning electron micrographs indicated that nanoclay exists in clusters of various sizes ranging from over 10 μm down to submicrometre scale. Nanoclay clusters larger than 1·5 μm, were analysed by digital image processing on the scanning electron micrographs taken along the part's radius. The dispersion of nanoclay smaller than 1·5 μm was quantified by compositional analysis via wavelength dispersive spectrometry (WDS). Distribution of nanoclay clusters larger than 1·5 μm was found to be approximately constant along the radius with an average value of 1·4% by volume. Similarly, nanoclay clusters smaller than 1·5 μm were found to be distributed evenly with an average value of 0·41 wt-%. To investigate the effect of nanoclay on thermo-mechanical properties, glass transition temperature of moulded samples was measured under oscillatory shear. At the current dispersion state, the glass transition temperature improved 11% with the addition of nanoclay.

Keywords: Nanoclay, Resin transfer moulding, Electron microprobe analysis

Introduction

Nanoclay has been receiving considerable interest from researchers following its introduction as a reinforcing agent for polymers in the early 1990s.[1–3] The current state of the research on the effects and utility of nanoclay was recently reviewed by Ahmadi *et al.*[4] Researchers have long tried to achieve superior thermo-mechanical and barrier properties with the incorporation of nanoclay into the polymer matrix.[5–8] For instance, Abot *et al.*[5] investigated the effectiveness of two different types of nanoclay, Nanomer I.28E and Cloisite 30B, in epoxy matrix. These nanoclay types were mechanically mixed into epoxy matrix at loadings ranging from 0 to 20% by weight. After observing the increase in gallery spacing for Nanomer I.28E and exfoliation for Cloisite 30B by X-ray diffractometry, the authors elucidated possible improvements in thermo-mechanical properties through uniaxial tension and dynamic mechanical analysis. Despite the existence of intercalated and exfoliated nanoclay, tensile strength and glass transition temperature were observed to deteriorate as much as 28% and 15%, respectively. However, over the range of nanoclay loading, stiffness was reported to increase by 30%. Abot *et al.*[5] also reported the existence of nanoclay clusters with sizes larger than 10 μm as indicated by scanning electron micrographs taken at low magnification. Although intercalated and exfoliated nanoclay may exist in the epoxy matrix, the effect of large nanoclay clusters may dominate the overall behaviour of the composite parts, thus resulting in improved stiffnesses at the expense of a considerable reduction in strength.

The practical challenge in fabricating nanoclay reinforced composites with improved performance is the dispersion of nanoclay in the polymer matrix, such that the cluster structures are broken down, exfoliated and distributed homogenously throughout the medium. As a result of the strong nanoscale forces[9] attracting nanoclay platelets to each other, obtaining fully exfoliated structures is often problematic. Solution blending, melt blending and *in situ* polymerisation have

School of Aerospace and Mechanical Engineering, University of Oklahoma, Norman, OK 73019, USA

*Corresponding author, email altan@ou.edu

Published by Maney on behalf of the Institute
Accepted 18 October 2004
DOI 10.1179/174328904X4918

been the primary methods to introduce nanoclay into the polymer.[4] However, regardless of the method used, nanoclay is first mixed with a host liquid. Several methods for mixing the nanoclay, including shear mixing[5–8] and ultrasonic mixing[6] have been implemented. Among such studies, a three-roll mill machine was used by Yasmin *et al.*[10] to mix the nanoclay into the epoxy matrix. Based on X-ray diffractometry and transmission electron microscopy analyses, Yasmin *et al.*[10] reported an increased degree of intercalation for longer mixing times with the three-roll mill machine. However, expected improvements in performance could not be achieved.

Traditionally, the dispersion of nanoclay in polymer matrices is quantified using transmission electron microscopy (TEM)[2,3,8,11,12] and X-ray diffractometry (XRD).[1–3,6,8,11,12] As a result of its high magnification, transmission electron microscopy can be utilised to image individual platelets. Based on these images, qualitative analysis on the state of dispersion can be made. On the other hand, X-ray diffractometry involves sending a well characterised X-ray on to the surface of interest and determining the intensity of the reflected energies. When the Bragg's condition is satisfied, the intensity registers a peak, indicating the gallery spacing of the nanoclay platelets. The increase in the gallery spacing of nanoclay in nanocomposite is most often attributed to intercalation, whereas disappearance of intensity peaks is often attributed to exfoliation. These methods, however, have certain shortcomings. For instance, as stated by Kornmann *et al.*,[13] in X-ray diffractometry, broad gallery spacing distribution may lead to indistinguishable intensity peaks which may yield inaccurate results. Transmission electron microscopy on the other hand, probes a very small area, thus the results may not be representative of the whole sample.[14]

In the current work, the authors present a novel method to characterise the state of nanoclay dispersion in moulded glass/nanoclay/epoxy composites. In this method, nanoclay clusters larger than 1·5 μm are identified by performing digital image analysis on SEM images of the composite cross-section. The remaining nanoclay, i.e. nanoclay smaller than 1·5 μm is quantified via wavelength dispersive spectrometry (WDS). Having established the state of dispersion, the authors assessed the improvement in glass transition temperature by dynamic mechanical analysis.

Experimental studies

Composite parts to be used in the present study were fabricated by resin transfer moulding (RTM) via a custom made moulding set-up depicted in Fig. 1. Two stainless steel cylinders on the set-up served as reservoirs for the resin (Epon 815C; Shell Chemicals) and curing agent (Epi-cure 3282; Shell Chemicals), respectively. The internal diameters of these two cylinders were machined to 55·5 and 25·5 mm for the resin and the curing agent, respectively, such that the required mixing ratio of 4·7 : 1 was achieved. The resin and the curing agent were forced to flow out of the reservoirs via a plunger arrangement operated by a 40-ton hydraulic press. The steady motion of the hydraulic press provided a constant volumetric flowrate of $5{\cdot}8 \times 10^{-6}$ m^3 s^{-1} for the resin-curing agent mixture. The outflows from the cylinders were merged

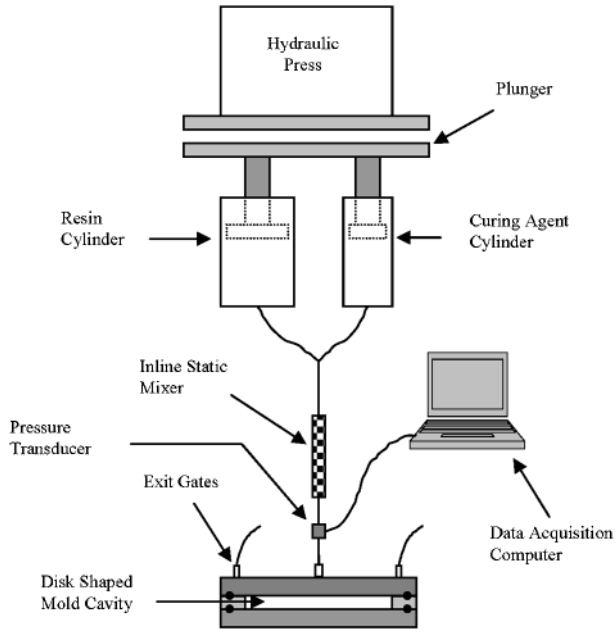

1 Experimental moulding set-up used to fabricate neat epoxy, composite and nanocomposite discs

by a t-connector and passed through an inline static mixer with 32 alternating helical mixing units, which provided thorough mixing of resin and curing agent. The mixture then entered the mould through a 6·4 mm diameter inlet gate located at the centre of the mould cavity. The mould cavity was formed by placing a 3·2 mm thick spacer plate with a 152·4 mm diameter circle cut out at its centre, between two aluminium mould walls. A set of o-rings on both mould walls prevented leakage and enabled application of the post-fill packing pressure. The resin/curing agent mixture was injected into the mould cavity until the mixture emerged from the four exit gates placed symmetrically on the top mould wall. Application of post-fill packing pressure was shown to improve the performance of resin transfer moulded parts by Olivero *et al.*[15] After filling was completed and exit gates had been clamped, the press was operated for an additional second for the application of post-fill packing pressure. Following the application of post-fill packing pressure, the inlet was clamped and the mould assembly removed for curing. Curing was carried out at room temperature for 2 days until the discs became rigid enough to be de-moulded.

Three sets of discs were moulded by the aforementioned method. The first set was fabricated without reinforcement. This set will be referred to as 'neat epoxy'. The second set was fabricated by placing eight layers of chopped strand glass fibre preforms into the mould cavity before moulding. The parts manufactured as such will be referred to as 'composite'. These composite parts have a fibre volume fraction of approximately 17%. In addition to having glass fibre reinforcements the same as the second set, 1·7 wt-% nanoclay was introduced to the third set.

The nanoclay used in the present study was Cloisite 25A (Southern Clay Products, TX, USA). A mechanical mixer was used to mix the nanoclay with the resin. As the resin started mixing, the proper amount of nanoclay was gradually added and mixing continued for 15 min. At the end of the mixing period, the suspension was left

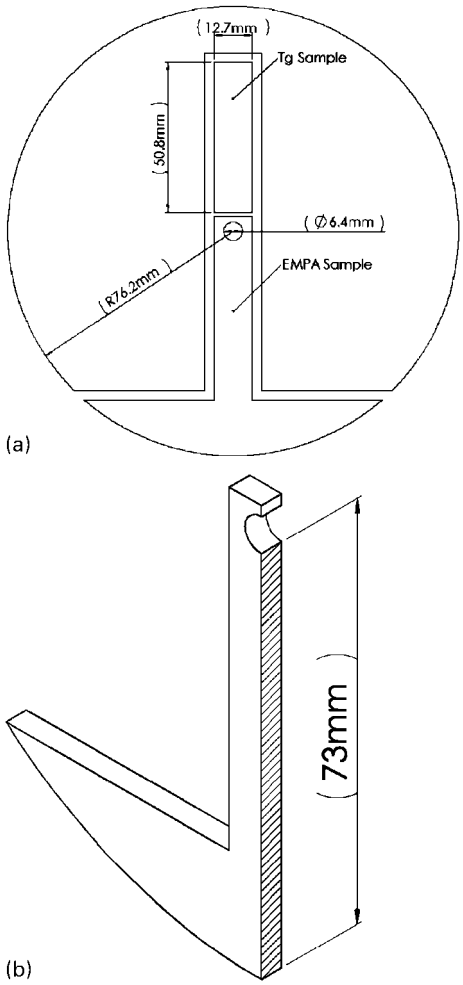

2 *a* Spatial distribution of samples cut from fabricated discs; *b* through-thickness cross-section utilised for quantification of dispersion

for degassing for 1 h. After degassing, air pockets were not seen as the mixture was loaded into the reservoir. This third set of discs will be referred to as 'nanocomposite'. It should be noted that the resin used in fabricating the neat epoxy and composite discs were also mixed and degassed under the same circumstances as the nanocomposite to eliminate any influence of mixing of epoxy on the thermo-mechanical properties.

Samples to be used for dispersion characterisation and thermo-mechanical analysis were cut out of the fabricated neat epoxy, composite and nanocomposite discs using a milling machine. The spatial distribution of the samples to be used for analyses is depicted in Fig. 2. The sample marked as EMPA was used in dispersion characterisation by electron microprobe analyser (EMPA). EMPA embodies a scanning electron microscope (SEM), an energy dispersive X-ray analyser and five wavelength dispersive spectrometers, which enable simultaneous SEM imaging and precise compositional analysis. Initial results from the scanning electron micrographs indicated that the nanoclay exists in the form of clusters of various sizes. Further observation of the microstructure at various magnifications revealed that there was a continuum of cluster sizes ranging from over 10 μm down to nanometer scale. A representative SEM image of the nanocomposite microstructure is depicted in Fig. 3. For the detailed analysis of dispersion

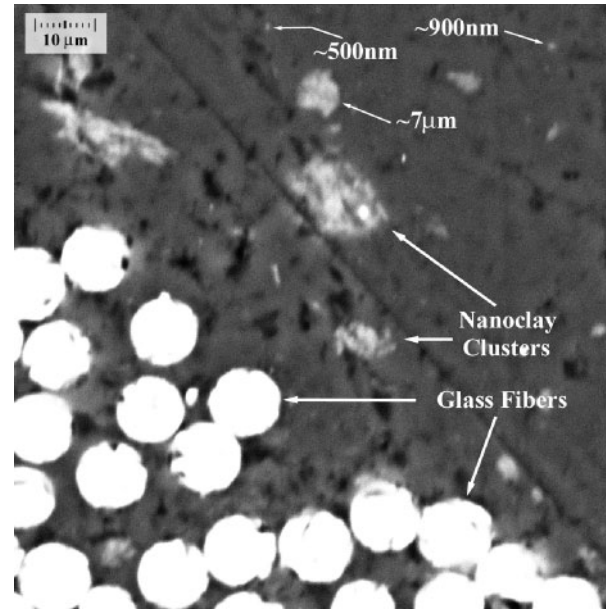

3 Representative SEM image of microstructure of nanocomposite disc taken at 750× magnification; different sizes of nanoclay clusters and glass fibres are depicted

of nanoclay along the radius of the disc, the nanoclay clusters larger than 1·5 μm were analysed by performing digital image analysis on scanning electron micrographs obtained at 50× magnification. Clusters smaller than 1·5 μm (i.e. those that could not be identified by digital image analysis) were analysed by wavelength dispersive spectrometry.

SEM images used in the image analysis were captured along the radius of the nanocomposite sample at 4 mm radial intervals. These images were then thresholded for the grey scale of the nanoclay clusters using UTSCHA Image Tool software. After thresholding, the images often had artefacts owing to the fibre bundles. These artefacts were eliminated by applying a series of morphological filters on the thresholded images. Thus, the final binary image only involved nanoclay clusters that were larger than 1·5 μm which is the size of one pixel at the given magnification. The initial captured image and final filtered image used in the analysis are depicted in Fig. 4.

Nanoclay clusters smaller than 1·5 μm were detected by wavelength dispersive spectrometry (WDS). After several trials, the spot diameter and beam current for the analysis was chosen to be 20 μm and 5 nA, respectively, to avoid beam damage on the surface. Under this beam condition, 2 min analysis time per location was found to yield sufficient accuracy as justified by 3σ minimum detection limits for the elements considered. The constituent elements of Cloisite 25A were determined by energy dispersive X-ray analysis (EDXA), the spectrum of which is shown in Fig. 5. The intensity peaks corresponding to characteristic X-rays indicated the constituting elements as magnesium, aluminium, silicon and iron. These elements were targeted in the wavelength dispersive spectrometry (WDS) analysis. The microbeam was positioned at discrete locations along the radius at 0·5 mm intervals, and the nanoclay content of each location was determined.

The glass transition temperature was measured under oscillatory shear on rectangular torsional samples using

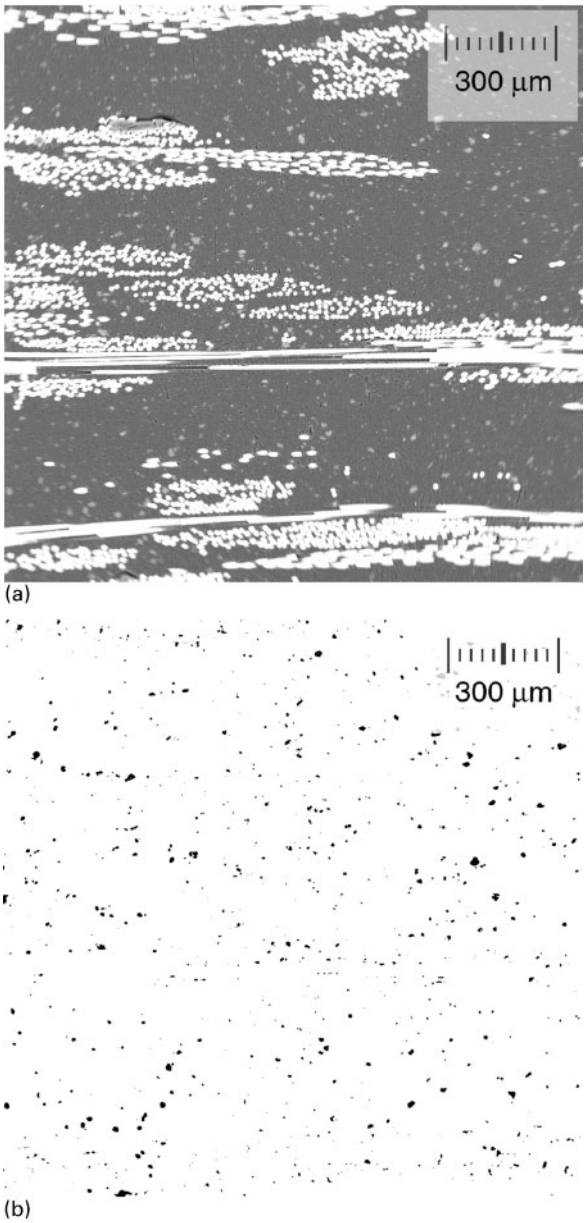

4 *a* As captured SEM image used in quantification of microscale dispersion; *b* same image after processing for identification of nanoclay clusters

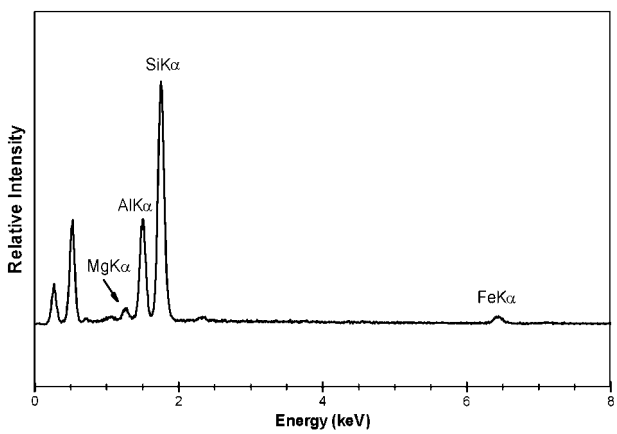

5 Energy dispersive X-ray spectrum of Cloisite 25A

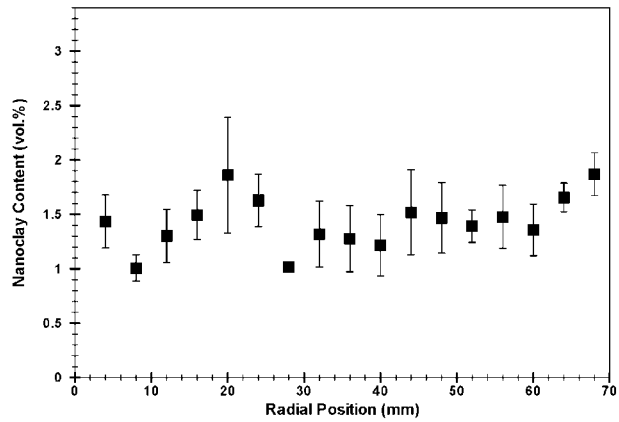

6 Radial distribution of nanoclay clusters dispersed to microscale; nanoclay content is obtained from digital image analysis

a RDAIII (Rheometrics Digital Analyzer) rheometer. Temperature was increased at a rate of 1°C min^{-1} from ambient temperature up to 121°C during which the sample was deformed under torsion at 1 Hz frequency. The glass transition temperature was determined using two commonly used methods. The first method is recommended by the American Society for Testing and Materials (ASTM) and involves determination of the temperature at which the storage modulus (G') drops drastically. The second method reports the glass transition temperature as the temperature at which the loss modulus (G'') displays a maximum.

Results

The dispersion characterisation of nanometer scale particles was performed by electron microprobe analysis (EMPA), which is composed of two primary components: scanning electron microscopy (SEM) and compositional analysis. As an initial attempt to identify nanoclay particles, scanning electron micrographs of a radial sample cut from the nanocomposite disc were analysed at various magnifications. These revealed that the microstructure displays a continuum of nanoclay cluster sizes. Hence for a thorough analysis, dispersion should be investigated in two phases: (a) microscale dispersion and (b) nanoscale dispersion. Microscale dispersion is defined here as clusters that are visible in SEM images taken at 50× magnification, which corresponds to nanoclay clusters larger than 1·5 μm. To quantify the dispersion in microscale, 50× magnification back scattered images of the surface were captured at 4 mm intervals along the radius for the moulded nanocomposite at 20 kV accelerating voltage. Captured images were subjected to a thresholding process and converted into binary images. To eliminate the artefacts introduced owing to the glass fibre/matrix interface, the binary images were subjected to a series of morphological filters. This process was repeated five times for each image to account for uncertainties introduced by the thresholding process. The resulting images were analysed for the volume fraction of nanoclay. The image analysis results are depicted in Fig. 6 together with 95% confidence interval error bars. The variation in the distribution of the nanoclay content at the microscale along the radius of the nanocomposite

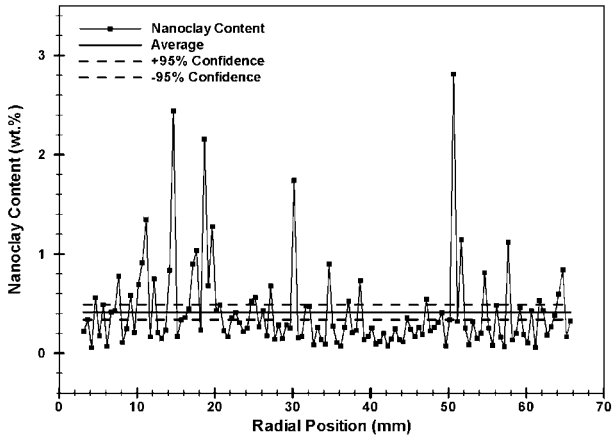

7 Radial distribution of nanoclay clusters dispersed to nanoscale; nanoclay content is obtained by wavelength dispersive spectrometry (WDS)

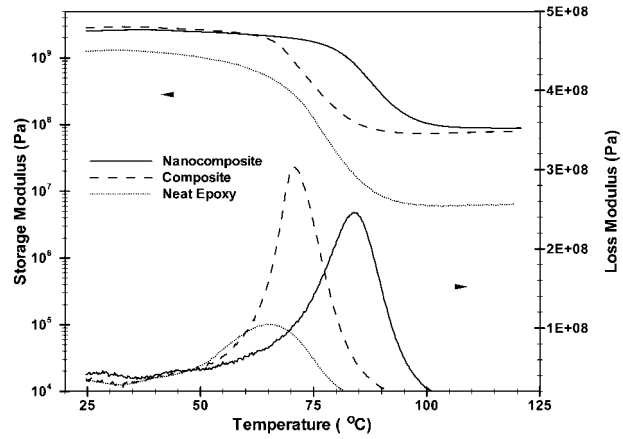

8 Evolution of storage (G') and loss moduli (G'') with temperature; G' and G'' variations are used in determining glass transition temperature

was observed to be insignificant. The average volume fraction of the microscale dispersion of nanoclay clusters was determined as 1·4%. The amount of nanoclay clusters determined through image analysis was not converted to weight fraction using the specific gravity specified by the manufacturer since the degree of compression of the nanoclay clusters and thus the effective densities were not known.

Nanoscale dispersion, i.e. nanoclay clusters smaller than 1·5 μm were accounted for by wavelength dispersive spectrometry (WDS). Regions of 20 μm diameter were analysed along the radius of the nanocomposite disc at 0·5 mm intervals. Special attention was paid to the choice of analytical volume, not to include nanoclay clusters larger than 1·5 μm, thus eliminating nanoclay accounted for by the image analysis. The results of nanoscale dispersion analysis by WDS are depicted in Fig. 7. Similar to microscale dispersion, particles dispersed down to nanoscale do not display a definite trend along the radius. This finding indicates that the flow path between the glass fibre preforms is wide enough not to cause filtration of the nanoclay in the flow direction. The average weight fraction of particles of nanoscale dispersion was determined to be 0·41%. Considering the initial loading of 1·7 wt-%, it can be concluded that approximately 24% of the nanoclay is dispersed to particle sizes below 1·5 μm. For the given beam condition and counting times, 3σ minimum detection limit (3σ MDL) was determined for each of the elements analysed. For magnesium, aluminium, silicon and iron, the MDLs were calculated as 0·02, 0·02, 0·03 and 0·04%, respectively. Evidently, throughout the WDS analyses, the peak to background intensity ratio and counting times were adequate for the accurate determination of nanoclay content.

Compared to TEM and XRD, the method developed in the present study provides information on the degree of dispersion at two different scales over a much larger area. However, neither digital image analysis nor wavelength dispersive spectrometry determines the state of exfoliation of the individual nanoclay platelets. The glass transition temperature of polymer composites most of the time indicates the structural integrity of the polymer chains. Therefore, if parts of the nanoclay platelets are exfoliated at the molecular level, they would cause an increase in the glass transition temperature. For instance, Ratna *et al.*[16] observed a 10·5% increase in glass transition temperature of epoxy resin with the addition of 5 wt-% organoclay. To determine the change in glass transition temperature because of glass fibre reinforcement and nanoclay, dynamic mechanical analysis was implemented on the samples cut from the neat epoxy, composite and nanocomposite discs. Representative curves for the evolution of storage and loss moduli for neat epoxy, composite and nanocomposite samples are depicted in Fig. 8. These curves were used to determine the glass transition temperatures using two methods, ASTM method and peak loss modulus method, which are depicted in Fig. 9. The improvement in glass transition temperature owing to the addition of glass reinforcement is observed to be 7·8 and 15·2% when determined by ASTM and peak loss modulus methods, respectively. Nanoclay reinforcement further improves the glass transition temperature by 11·7%, making the overall improvement 20·4% over the neat epoxy.

Concluding remarks

A novel method is introduced that implements electron microprobe analysis (EMPA) for the characterisation of nanoclay dispersion in an epoxy matrix. The dispersion of microscale clusters (i.e. clusters >1·5 μm) is identified by performing digital image analysis on SEM images of the cross-section. The remaining nanoclay (i.e. clusters

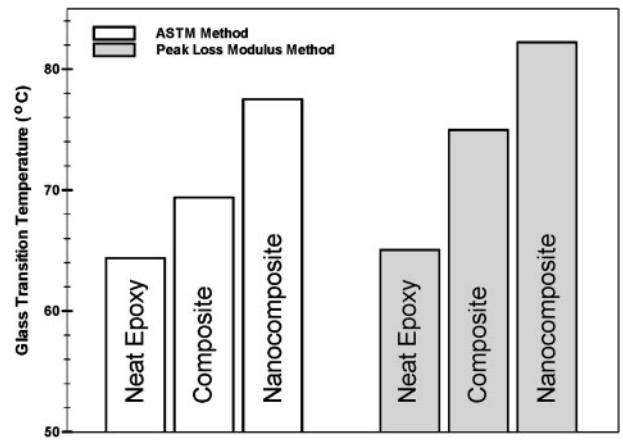

9 Glass transition temperatures for neat epoxy, composite and nanocomposite samples as determined by ASTM and peak loss modulus methods

<1·5 μm) is quantified using wavelength dispersive spectrometry (WDS). The application of this method is demonstrated on a resin transfer moulded glass/nanoclay/epoxy disc. It was determined that 24% of the initial nanoclay loading of 1·7 wt-% is dispersed to clusters smaller than 1·5 μm. The glass transition temperature of neat epoxy, composite and nanocomposite samples is measured by dynamic mechanical analysis. The improvement of the glass transition temperature by 11% owing to the addition of nanoclay may indicate the existence of exfoliated nanoclay within the matrix.

Acknowledgements

This is a revised version of a presentation made at the PPS20 event organised by the Polymer Processing Society on 20–24 June 2004 in Akron, OH, USA.

References

1. A. Usuki, M. Kawasumi, Y. Kojima, A. Okada, T. Kurauchi and O. Kamigaito: *J. Mater. Res.*, 1993, **8**, 1174–1178.
2. A. Usuki, Y. Kojima, M. Kawasumi, A. Okada, Y. Fukushima, T. Kurauchi and O. Kamigaito: *J. Mater. Res.*, 1993, **8**, 1179–1184.
3. Y. Kojima, A. Usuki, M. Kawasumi, A. Okada, Y. Fukushima, T. Kurauchi and O. Kamigaito: *J. Mater. Res.*, 1993, **8**, 1185–1189.
4. S. J. Ahmadi, Y. D. Huang and W. Li: *J. Mater. Sci.*, 2004, **39**, 1919–1925.
5. J. L. Abot, A. Yasmin and I. M. Daniel: *Mater. Res. Soc. Symp. Proc.*, 2003, **740**, 162–177.
6. I. Isik, U. Yilmazer and G. Bayram: *Polymer*, 2003, **44**, 6371–6377.
7. T. Lan and J. Pinnavaia: *Chem. Mater.*, 1994, **6**, 2216–2219.
8. A. J. Kinloch and A. C. Taylor: *J. Mater. Sci. Lett.*, 2003, **22**, 1439–1441.
9. N. J. Wagner and J. B. Bender: *MRS Bull.*, 2004, **29**, 100–106.
10. A. Yasmin, J. L. Abot and I. M. Daniel: *Mater. Res. Soc. Symp. Proc.*, 2003, **740**, 75–80.
11. M. Okamoto, S. Morita, Y. H. Kim, T. Kotaka and H. Tateyama: *Polymer*, 2001, **42**, 1201–1206.
12. J. H. Park and S. C. Jana: *Polymer*, 2003, **44**, 2091–2100.
13. X. Kornmann, H. Lindberg and L. A. Berlund: *Polymer*, 2001, **42**, 1303–1310.
14. R. Wagener and T. J. G. Reisinger: *Polymer*, 2003, **44**, 7513–7518.
15. K. A. Olivero, H. J. Barraza, E. A. O'Rear and M. C. Altan: *J. Compos. Mater.*, 2002, **36**, 2011–2028.
16. D. Ratna, O. Becker, R. Krishnamurthy, G. P. Simon and R. J. Varley: *Polymer*, 2003, **44**, 7449–7457.